doi.org/10.36721/PJPS.2026.39.4.REG.14899.1

miR-193a-5p carried by ferric oxide nanoparticles interferes with the TGF-β1/Smad signaling pathway and promotes pyroptosis in gastric cancer cells

Huijuan Yu[#], Ye Lu[#], Ziqin Chen and Xiaoshuang Du*
Department of Radiotherapy, Huai'an Hospital Affiliated to Yangzhou University (The Fifth People's Hospital of Huai'an), Huai'an, Jiangsu, China

Abstracts: **Background**: The transforming growth factor -β1 (TGF-β1) /Smad signaling pathway plays a critical role in gastric cancer pathogenesis. **Objective**: This study investigates how microRNA-193a-5p (miR-193a-5p) delivered by iron oxide nanoparticles (Fe_3O_4 nanoparticles, NPs) influences gastric cancer cell pyroptosis through TGF-β1/Smad signaling. **Methods**: The MiR-193a-5p-Fe_3O_4 NPs composite material was constructed to treat human gastric cancer cells MKN28. The control group, miR-193a-5p group, Fe_3O_4 NPs group, MiR-193a-5p-Fe_3O_4 NPs group and the combined treatment group of pathway inhibitors/activators were set up. Detect the expression of proteins related to cell proliferation, migration, apoptosis and pyroptosis. **Results**: miR-193a-5p-Fe_3O_4 NPs can significantly inhibit the proliferation and migration of gastric cancer cells, induce apoptosis and pyroptosis and down-regulate the activity of the TGF-β1/Smad pathway. The combination of TGF-β pathway inhibitor SB431542 can enhance the above effect, while the activator SIS-011381 can partially reverse this effect. **Conclusion**: miR-193a-5p-Fe_3O_4 NPs promote pyroptosis of gastric cancer cells by inhibiting the TGF-β1/Smad signaling pathway. Its combination with SB431542 has a synergistic anti-tumor effect, providing a new idea for the treatment of gastric cancer.

Keywords: Ferric oxide; Gastric cancer; miR-193a-5p; Nanoparticles; Pyroptosis; TGF-β1/Smad

Submitted on 24-07-2025 – Revised on 04-11-2025 – Accepted on 13-11-2025

INTRODUCTION

Gastric cancer is one of the most common malignant tumors worldwide and its high mortality rate is closely associated with tumor invasion, metastasis and therapy resistance. Therefore, exploring new therapeutic targets and strategies is of utmost importance. Pyroptosis is a form of programmed cell death mediated by Gasdermin family proteins, characterized by cell swelling, membrane pore formation and the release of inflammatory factors. Recent studies have shown that inducing pyroptosis in tumor cells can effectively inhibit tumor growth and activate anti-tumor immune responses, making it a highly promising new direction for cancer treatment.

MicroRNA-193a-5p (miR-193a-5p) has been demonstrated to act as a tumor suppressor in various cancers (Wang *et al*., 2022). Studies (Baghbanzadeh *et al*., 2022) have indicated that in liver cancer, miR-193a-5p may suppress the malignant transformation of hepatocellular carcinoma cells by targeting genes such as HOXC9. In gastric cancer, its downregulation is associated with malignant progression (Sun *et al*., 2021). Previous research has primarily focused on how miR-193a-5p inhibits the growth and development of gastric cancer cells by regulating target genes such as E2F1, ERBB4 and MCL1 (Carpi *et al*., 2020). However, whether and how it participates in regulating pyroptosis in gastric cancer cells remains unclear. Other studies suggest that miR-193a-5p can target the NLRP3 inflammasome, a key component in initiating the classical pyroptosis pathway (Feng *et al*., 2024). This provides a potential theoretical clue that miR-193a-5p may inhibit gastric cancer by regulating pyroptosis.

The TGF-β signaling regulates many biological processes (Peng *et al*., 2022). In colorectal cancer (Yu *et al*., 2021), miR-193a-5p may inhibit TGF-β signaling by inhibiting SMAD3 expression, thereby inhibiting colorectal cancer cells. In addition, in breast cancer, miR-193a-5p may regulate TGF-β signaling by targeting genes such as TGFBR3 (TGF-beta receptor type III), thereby affecting the behaviors of breast cancer cells (Zhang *et al*., 2020). Although regulating TGF-β can be involved in the treatment of various cancers, there are few research reports on the treatment of gastric cancer. In lung cancer, miR-193a-5p inhibits TGF-β1 expression by targeting mRNA of TGF-β1, thereby inhibiting the activities of lung cancer cells (Xiang *et al*., 2020). In gastric cancer, miR-193a-5p inhibits the activities of gastric cancer cells by inhibiting Smad3, a key molecule in TGF-β1/Smad signal (Zhang *et al*., 2022). In addition, miR-193a-5p can also target and regulate the expression of NLRP3 inflammasome, thereby inhibiting pyroptosis of tumor cells (Zhang *et al*., 2020). In gastric cancer, pyroptosis may be related to tumor growth, response to anticancer therapy and immune response. Researchers are studying the role of pyroptosis in the development of cancer and whether this method of cell death can be exploited to develop new treatment strategies.

**Corresponding author:* e-mail: shuang_01990@163.com
[#]These authors contributed equally and are the co-first authors.

Ferric oxide (Fe_3O_4) nanoparticles are a kind of nanoparticles with special properties and wide applications (Mehta *et al*., 2022). Studies have reported that Fe_3O_4 NPs have strong magnetism. Under the action of an external alternating magnetic field, they can generate local heat and are used in magnetothermal therapy, that is, to guide the nanoparticles to the tumor site and then use external alternating magnetic fields to Variable magnetic fields produce localized thermotherapeutic effects and are used for cancer treatment (Qi *et al*., 2021). Compared with some other metal nanomaterials, Fe_3O_4 nanoparticles generally have better biocompatibility, which makes their applications in the biomedical field more promising (Piro *et al*., 2023). In addition, the surface of Fe_3O_4 NPs can be chemically modified to give them specific functions. By introducing different molecules on the surface modification, nanoparticles can achieve functions such as targeted delivery and drug release control and due to their surface modification capabilities, they can be used as carriers for drug delivery (Rouhani and Singh, 2020). Drugs can be adsorbed on the surface of nanoparticles or immobilized through physical or chemical methods to achieve targeted delivery and controlled release of drugs.

Therefore, loading miRNA on nanoparticles can improve the targeted delivery performance of miRNA and deliver miRNA to tumor cells more accurately. Studies have found (Hill and Tran, 2021) that miRNA is easily degraded in the body and loading it on nanoparticles can protect miRNA from degradation, thereby prolonging its existence time in the body and increasing its therapeutic effect. At the same time, nanoparticles can be designed as carriers that can control the release of miRNA. This allows miRNA to be released when and where needed, improving the accuracy and effectiveness of treatment (Diener *et al*., 2022). This method combines the advantages of nanotechnology and gene therapy and can bring more potential applications and research value to areas such as cancer treatment, which can provide theoretical support for exploration of new treatment strategies for gastric cancer.

Based on the above background, we propose the following research hypothesis: Fe_3O_4 NPs-loaded miR-193a-5p can effectively target gastric cancer cells and, by inhibiting the TGF-β1/Smad signaling pathway, subsequently upregulate the expression of the key pyroptosis execution protein GSDMD-N, ultimately inducing pyroptosis in gastric cancer cells. This study aims to validate this hypothesis and provide a solid experimental foundation for developing novel gastric cancer treatment strategies based on nanotechnology and miRNA intervention.

MATERIALS AND METHODS

Experimental materials

Human gastric cancer cell line MKN28 (Shanghai Eniyan); MTT solution, SB431542 (Shanghai Yuanye); SRI-011381 (Hubei Aimeijie); NLRP-3 antibody (Wuhan Huamei); GSDMD-N antibody (Wuhan Boote); Inverted microscope (Shanghai Leica Microsystems); Scanning electron microscope (SEM) was purchased from Shanghai Carl Zeiss.

Cell culture and identification

The human gastric cancer cell line MKN28 was purchased from Shanghai Yisheng Biotechnology Co., Ltd. This cell line belongs to the intestinal subtype of gastric cancer with moderate differentiation. It is an internationally recognized classic model for gastric cancer research and can reasonably represent the most common clinical type of gastric cancer. Although gastric cancer exhibits significant heterogeneity, selecting this classic cell line helps establish a reliable foundation for initial mechanistic exploration and provides a reference for subsequent extended studies in different gastric cancer subtypes.

The cells were cultured in RPMI-1640 medium supplemented with 10% fetal bovine serum (FBS) and 1% penicillin-streptomycin in a constant temperature incubator at 37°C with 5% CO2. Cell line identity was authenticated by short tandem repeat (STR) analysis. Mycoplasma testing was performed regularly using a PCR-based mycoplasma detection kit to ensure all experiments used mycoplasma-negative cells. As a commercially purchased cell line was used in this study, which did not involve obtaining tissues directly from human subjects, additional approval from the institutional ethics committee was not required. All experimental procedures followed standard ethical norms for cell biology research.

Preparation of Fe_3O_4 nanoparticles

Weigh 10.9g $FeSO_4 \cdot 7H_2O$ and 4.0g $FeCl_3 \cdot 6H2O$ and dissolve them in 30 mL deionized water. Pour in nitrogen and add 2 mL hydrazine hydrate while stirring with a mechanical stirrer. Then add 35 mL concentrated ammonia dropwise to adjust the solution. The pH is 9. After stirring for 30 min, it was heated to 80℃ for 1 h. The reaction was stopped and a magnet was used for magnetic separation to remove supernatant and the lower solid was washed with deionized water, then with absolute ethanol and finally dried in vacuum. Dry at 60℃ for 12 hours to obtain Fe_3O_4 nanoparticles.

Preparation of miR-193a-5p-Fe_3O_4 NPs

On the basis of preparing Fe_3O_4 nanoparticles, biotin-avidin technology is used to connect miR-193a-5p to the nanoparticles. The miR-193a-5p-Fe_3O_4 nanoparticles are placed on the electron microscope sample stage and morphology and size of miR-193a-5p-Fe_3O_4 were observed under a transmitted electron microscope.

Determination of miR-193a-5p loading efficiency on Fe_3O_4 NPs

After conjugating miR-193a-5p to Fe_3O_4 NPs using biotin-avidin technology, the loading efficiency was

quantitatively analyzed by an ultrafiltration centrifugation-absorbance measurement method. The prepared miR-193a-5p-Fe_3O_4 NP complex solution was transferred to an ultrafiltration centrifuge tube (molecular weight cut-off: 100 kDa) and centrifuged at 4°C, 12,000 × g for 15 minutes. The supernatant containing free miR-193a-5p was collected. The absorbance of the free miR-193a-5p in the supernatant was measured at 260 nm using a microspectrophotometer and its concentration (C_free) was calculated based on a standard curve.

The loading efficiency was calculated according to the following formula: Loading efficiency (%) = [(W_total - W_free) / W_total] × 100%. Where W_total is the total mass of miR-193a-5p added during preparation and W_free is the mass of free miR-193a-5p measured after centrifugation. The measured loading efficiency of the prepared miR-193a-5p-Fe_3O_4 NP complexes in this study was 85.2 ± 3.7% (n=3).

Experimental methods

Cell grouping and transfection

Cells in the good-growth logarithmic phase were used for experiments. All treatment agents (miR-193a-5p mimic, Fe_3O_4 NPs and their complexes) were diluted to the specified working concentrations using serum-free RPMI-1640 medium before being added to the cell culture medium. The experimental groups and treatment conditions were as follows: MKN28 Group: Untreated blank control group; miR-193a-5p Group: Transfected with 50 nM miR-193a-5p mimic; Fe_3O_4 NPs Group: Co-incubated with Fe_3O_4 nanoparticles at a concentration of 100 μg/mL; miR-193a-5p-Fe_3O_4 NPs Group: Co-incubated with the complex of 50 nM miR-193a-5p loaded onto 100 μg/mL Fe_3O_4 NPs; SB431542 Group: Treated with 10 μM of the TGF-β receptor I inhibitor SB431542; SRI-011381 Group: Treated with 1 μM of the TGF-β pathway activator SRI-011381; miR-193a-5p-Fe_3O_4 NPs + SB431542 Group: Combination treatment (concentrations as above); miR-193a-5p-Fe_3O_4 NPs + SRI-011381 Group: Combination treatment (concentrations as above).

Proliferation assay and viability detection

MKN28 cells in the logarithmic growth phase were seeded into 96-well plates at a density of 2×10^3 cells per well, with 5 replicate wells set up for each group. After cell attachment (approximately 12 hours), the medium was replaced with fresh medium containing the different treatment factors. Following another 48 hours of culture, 20 μL of MTT solution (5 mg/mL, dissolved in PBS) was added to each well and the plates were incubated in the dark at 37°C for 4 hours. The supernatant in the wells was carefully aspirated and 150 μL of dimethyl sulfoxide (DMSO) was added to each well. The plates were then placed on a shaker and gently agitated for 10 minutes to fully dissolve the formed formazan crystals.

The absorbance of each well was measured at a wavelength of 570 nm using a microplate reader, with a reference wavelength of 690 nm used for correction. Cell viability was calculated according to the following formula:

Cell Viability (%) = [(Absorbance of Experimental Group - Absorbance of Blank Group) / (Absorbance of Control Group - Absorbance of Blank Group)] × 100%.
The experiment was independently repeated 3 times.

Cell scratch experiment

First, seed MKN28 cells evenly in a culture dish and allow to form a tight monolayer. Next, use a fine-tipped microinjection needle to gently make linear scratches in the cell monolayer. Wash with PBS, add culture medium and put back into the box to culture the cells. Scratch wound images were captured at the exact same location under a microscope at 0, 24 and 48 hours post-scratching. It could be observed that cells migrated from both edges of the scratch towards the gap, leading to wound closure.

Quantitative analysis of cell migration was performed using ImageJ software (National Institutes of Health, USA). The specific steps were as follows: the acquired images were imported into the software, calibrated by setting a uniform scale and the open wound area or width at each time point was measured. The cell migration rate was calculated using the following formula: Migration Rate (%) = [(Wound Area at 0h - Wound Area at T h) / Wound Area at 0h] × 100%. The experiment was independently repeated 3 times and all data are presented as mean ± standard deviation.

Apoptosis

After cultured for 24 hours, supernatant was discarded, washed with PBS solution, then digested with 0.25% trypsin and centrifuged to collect the cell pellet. Wash cells and then add 500μL of Binding Buffer solution (cell density is 1×106 cells/mL). Then add 5μL of Annexin V-FITC (Wuxi Bohe) under dark conditions and incubate. Add 5μL of propidium iodide (PI), incubate under the same conditions for 10 minutes and detect with flow cytometry (BD Company, USA).

All flow cytometry data were analyzed using a uniform gating strategy. First, a live cell gate (P1) was set on the forward scatter area (FSC-A) vs. side scatter area (SSC-A) dot plot to exclude debris. Subsequently, a single-cell gate (P2) was established using forward scatter area (FSC-A) vs. forward scatter height (FSC-H) to exclude cell aggregates. The total apoptosis rate was defined as the sum of the percentages of early apoptotic (Annexin V^+/PI^-) and late apoptotic (Annexin V^+/PI^+) cells within the P2 gate. The positions of the quadrant gates for all markers remained identical across all samples during analysis. The percentage of Annexin V^+/PI^+ cells was also recorded as an indicator associated with pyroptosis. This experiment was independently repeated three times.

PCR detection of TGF-β1 and Smad gene expression

MKN28 cells were ground and homogenized using liquid nitrogen and total mRNA was extracted and transcribed into cDNA. The analysis was performed by real-time PCR system analysis (Shanghai Unico) and GAPDH was selected as a reference. Relative levels were estimated using $2^{-\Delta\Delta Ct}$ method. Table 1 lists the primers and primer sequences.

Western blotting analysis of protein expression

Take MKN28 cells, extract total protein with TriZol reagent and detect the concentration. The electrophoresed total protein was heated to 100ºC and incubated for 5 min, then electrophoresed using an SDS-polyacrylamide gel (120 V, 100 min). Transfer separated proteins to PVDF membrane. To block, the membrane was incubated with NLRP-3, GSDMD-N antibody and GAPDH overnight at 4°C. The next day, incubate and wash the membrane three times and incubate with secondary antibody (1:10,000) for 1 hour (37ºC). Wash with PBS, repeat 3 times. All Western blotting bands were quantitatively analyzed for optical density using ImageJ software (National Institutes of Health, USA). The signal intensity of target proteins (such as NLRP-3 and GSDMD-N) was normalized to that of the internal reference protein GAPDH to correct for potential loading differences. The final data are expressed as the ratio of the grayscale value of the target protein to that of GAPDH.

Furthermore, all presented Western blotting images include the results of the loading control (i.e., GAPDH) to ensure comparable loading across all lanes and to demonstrate consistent protein transfer and detection efficiency throughout the experiment.

Statistical analysis

The data obtained in each of the above experiments were analyzed using SPSS26.0 and GraphPad Prism software. If there are no special requirements, $P<0.05$ is used as the test standard.

RESULTS

miR-193a-5p-Fe3O4 NPs were successfully prepared

The miR-193a-5p-Fe_3O_4 NPs composite was successfully synthesized using biotin-avidin conjugation. Transmission electron microscopy characterization revealed well-dispersed spherical nanoparticles with a mean diameter of 52.3 ± 4.7 nm (Fig. 1). Size distribution analysis confirmed the homogeneity of the prepared nanoparticles, with over 85% of particles falling within the 45-60 nm range. The uniform morphology and appropriate size distribution support the suitability of these nanoparticles for subsequent cellular experiments.

miR-193a-5p-Fe_3O_4 NPs can inhibit the activities of gastric cancer cells and induce apoptosis and pyroptosis and TGF-β1/Smad is involved

We first evaluated the biological effects of miR-193a-5p-Fe_3O_4 NPs on gastric cancer MKN28 cells. Functional assays demonstrated that treatment with miR-193a-5p-Fe_3O_4 NPs significantly reduced cell viability and inhibited migratory capacity compared to the Model group (Fig. 2A, B). In contrast, a marked increase in apoptosis was observed in the treated cells (Fig. 2C. Furthermore, to investigate the induction of pyroptosis, we examined the expression of key pyroptosis-related proteins. Western blot analysis showed a notable upregulation of NLRP-3 and GSDMD-N following miR-193a-5p-Fe_3O_4 NPs intervention, indicating the most significant activation of pyroptosis among the groups (Fig. 2D-F). To explore the potential mechanism, we analyzed the expression of genes within the TGF-β1/Smad pathway. Quantitative PCR results revealed a gradual down regulation in the expression levels of both TGF-β1 and Smad under various drug interventions, with the most pronounced decrease occurring in the miR-193a-5p-Fe_3O_4 NPs group (Fig. 2G). These findings collectively suggest that the inhibition of gastric cancer cell behaviors and the induction of apoptosis and pyroptosis by miR-193a-5p-Fe_3O_4 NPs may be mediated through the suppression of the TGF-β1/Smad pathway.

miR-193a-5p-Fe_3O_4 NPs inhibits TGF-β1/Smad signaling

To further validate the involvement of TGF-β1/Smad signaling in the observed effects, we conducted a series of mechanistic investigations. Initial assessment of TGF-β1 expression demonstrated that treatment with miR-193a-5p-Fe_3O_4NPs combined with SB431542 resulted in significantly down-regulated TGF-β1 levels, consistent with the trend observed in the SB431542 alone group (Fig. 3A). This synergistic suppression suggests that miR-193a-5p-Fe_3O_4 NPs can effectively mediate reduction of TGF-β1 levels in gastric cancer cells.

Subsequent evaluation of cellular responses revealed that the combination treatment of miR-193a-5p-Fe_3O_4 NPs and SB431542 produced the most substantial anti-tumor effects. Specifically, this combination group showed the lowest cell viability (Fig. 3B) and most inhibited migratory capacity (Fig. 3C) among all treatment conditions. Conversely, apoptosis rates reached their highest levels in this combination group (Fig. 3D), demonstrating a clear inverse relationship with the proliferation and migration findings. Further investigation into pyroptosis induction revealed that the expression levels of both NLRP-3 and GSDMD-N were elevated to their maximum extent under the combined intervention of miR-193a-5p-Fe_3O_4 NPs and SB431542 (Fig. 3E-G), indicating the most significant pyroptosis activation among all experimental groups. Importantly, the reversal of these effects by co-treatment with SRI-011381, a TGF-β pathway activator, provides compelling evidence that the observed anti-tumor activities are specifically mediated through TGF-β1/Smad signaling pathway inhibition.

Table 1: PCR primers and primer sequences.

Primers		Sequences
TGF-β1	*Forward primer*	5'-ACTTCTGGATGCTGGTGATTTG-3'
	Reverse primer	5'-GCTTCGCTGTGTGTTTTGTTCT-3'
Smad	*Forward primer*	5'-ACGGCAGGTCATCACTATTG-3'
	Reverse primer	5'-TGGATGCCACAGGATTCCAT-3'
GAPDH	*Forward primer*	5'-CATCACTGCCACCCAGAAGACTG-3'
	Reverse primer	5'-ATGCCAGTGAGCTTCCCGTTTCAG-3'

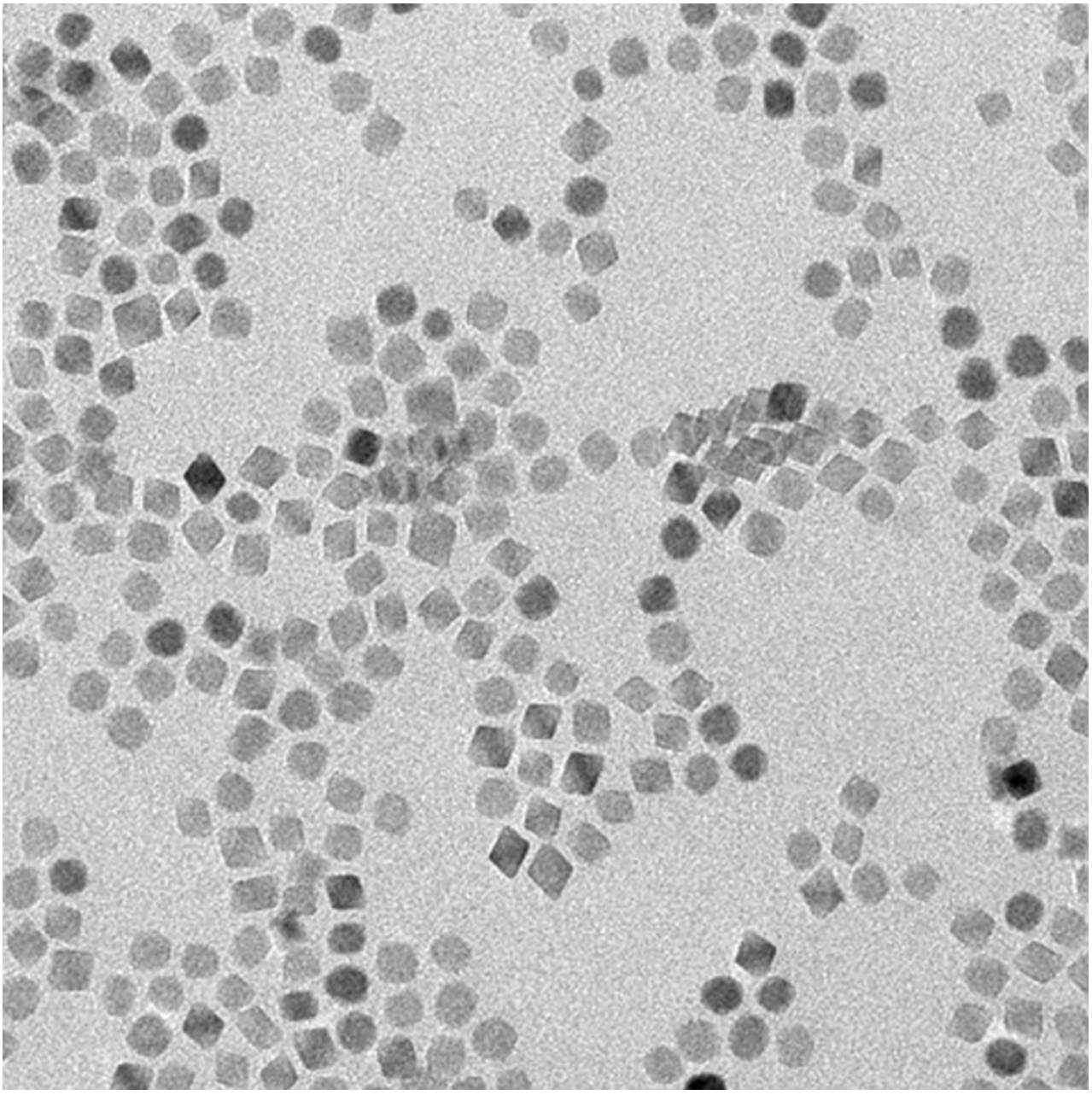

Fig. 1: Imaging and size distribution of miR-193a-5p-Fe_3O_4

DISCUSSION

This study successfully constructed the miR-193a-5p-Fe_3O_4 NP complex and demonstrated its ability to effectively induce pyroptosis in gastric cancer MKN28 cells by inhibiting the TGF-β1/Smad signaling pathway.

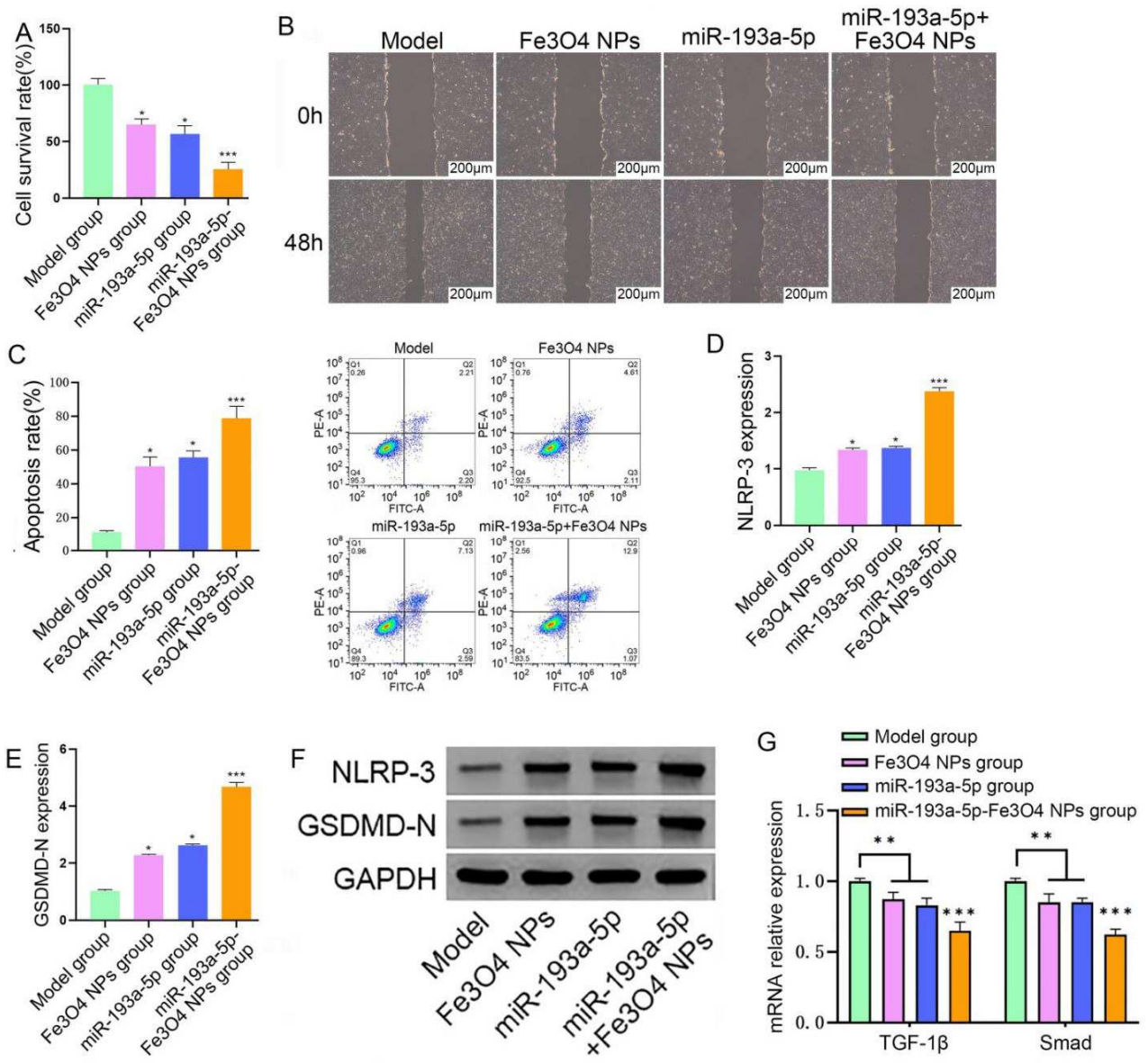

Fig. 2: Fe_3O_4 NPs-miR-193a-5p can inhibit the proliferation and migration of gastric cancer cells and induce apoptosis and pyroptosis.

Note: (A) MTT detects cell survival rate; (B) Cell scratch experiment detects cell migration; (C) Flow cytometry detects cell apoptosis rate; (D-F) WB detects cell char expression of death proteins NLRP-3 and GSDMD-N; (G).PCR detection of TGF-β1/Smad pathway protein expression; data are presented as mean ± standard deviation; compared with Model group, *P<0.05, **P<0.01, ***P<0.001.

This finding not only reveals a novel mechanism of miR-193a-5p in gastric cancer treatment but also highlights the unique advantages of nanocarriers in enhancing the efficiency of gene therapy.

From a mechanistic perspective, previous studies have shown (Wang *et al*., 2022) that miR-193a-5p inhibits cancer cell proliferation by regulating the PI3K/Akt signaling pathway and forming RNA-RNA complexes. Other studies (Pashirzad *et al*., 2021; Wen *et al*., 2022) have found that miR-193a-5p can prevent the normal translation process of MAPK and ERK mRNAs, reduce their protein synthesis, thereby affecting the normal activation of the MAPK/ERK signaling pathway and suppressing cancer development. This study, for the first time, confirms that miR-193a-5p can induce pyroptosis in gastric cancer by regulating the TGF-β1/Smad pathway. Although the expected therapeutic effects were observed, miR-193a-5p may simultaneously regulate multiple target genes. This multi-target characteristic could potentially lead to synergistic therapeutic effects but may also cause unforeseen adverse reactions, which require focused attention in subsequent research.

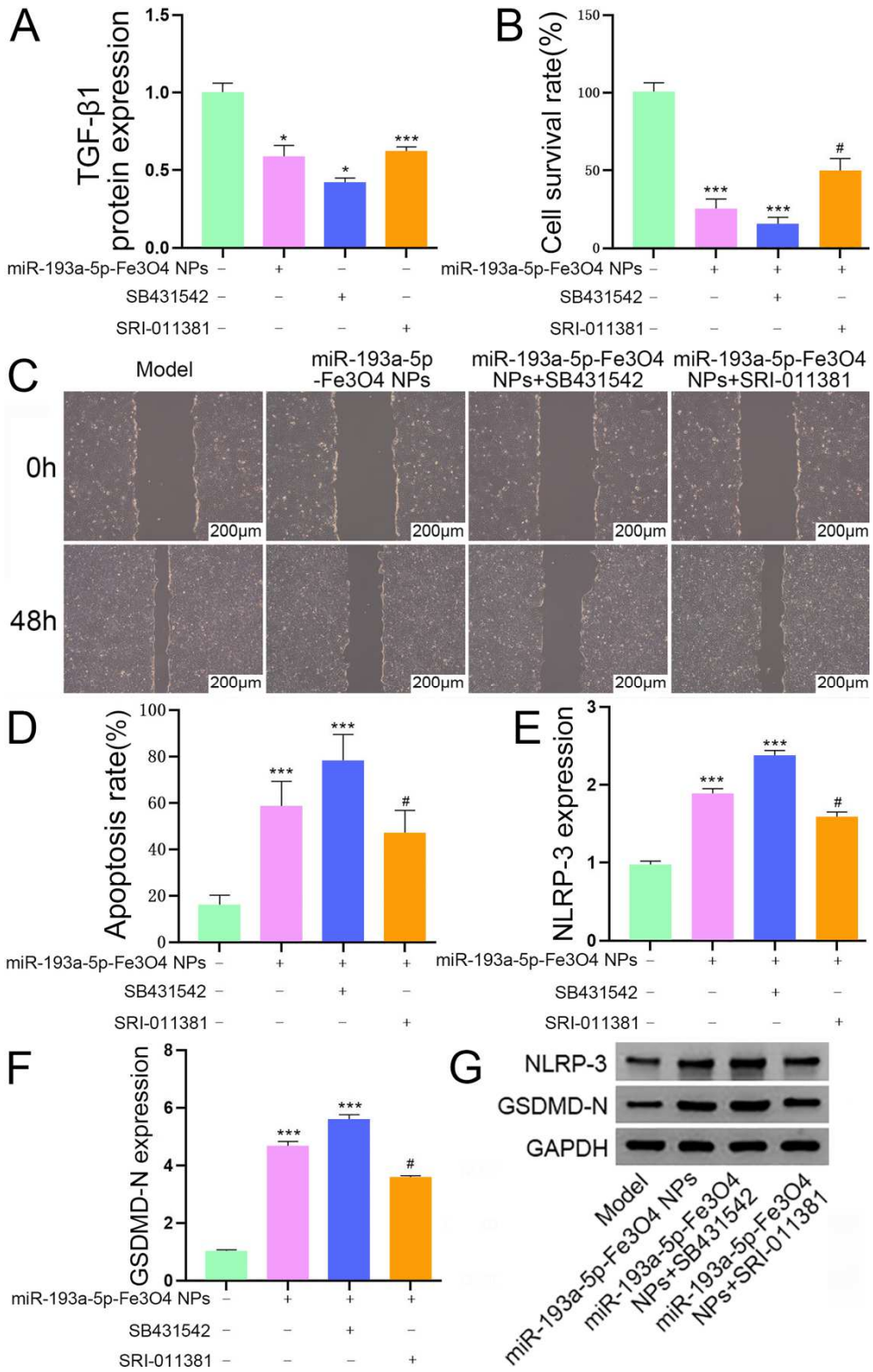

Fig. 3: miR-193a-5p-Fe_3O_4 NPs inhibits the proliferation and migration of gastric cancer cells and induces apoptosis and pyroptosis, which is related to inhibiting the activation of the TGF-β1/Smad signaling pathway.

Note: (A) WB detects TGF-β1 protein expression; (B) MTT detects cell survival rate; (C) Cell scratch experiment detects cell migration; (D) Flow cytometry detects cell apoptosis rate; (E-G) Expression of pyroptosis proteins NLRP-3 and GSDMD-N; data are presented as mean ± standard deviation; compared with Model group, *P<0.05, ***P<0.001; compared with miR-193a-5p-Fe3O4 NPs group, # P<0.05.

In terms of therapeutic strategies, although miR-193a-5p, as an anti-cancer gene, holds broad application prospects, nucleases can degrade miRNA *in-vivo*, shortening its half-life. Additionally, due to its negative charge and low molecular weight, miRNA struggles to cross cell membranes and enter target cells, often limiting its local stability and efficacy in therapy (Han *et al*., 2021). Therefore, finding a carrier to address these issues is necessary. Using Fe_3O_4 NPs as a drug carrier can not only protect miRNA from degradation and enhance its stability but also improve the cellular uptake efficiency of miRNA *in-vivo*, contributing to better therapeutic outcomes. Furthermore, Fe_3O_4 NPs can achieve targeted delivery to tumor cells by modifying their surface properties or adding specific targeting molecules, thereby improving the therapeutic effect of miRNA (Albalawi *et al*., 2021; Gokduman and Gok, 2020). Thus, we successfully prepared the miR-193a-5p-Fe_3O_4 NP composite material for gastric cancer treatment. However, translating this strategy into clinical practice still faces significant challenges. In addition to further evaluating the long-term biosafety of nanomaterials, achieving tumor-specific delivery in the complex *in-vivo* environment remains an urgent problem to solve. Current *in-vitro* models cannot fully replicate the complexity of the tumor microenvironment, including factors such as vascular barriers and interactions with immune cells.

Based on the above considerations, we recommend that future research focus on the following directions: First, it is essential to validate the anti-tumor efficacy and biosafety of miR-193a-5p-Fe_3O_4 NPs in animal models, as this is a necessary step toward clinical translation. Second, systematic evaluation of the off-target effects of miR-193a-5p using technologies such as transcriptomics should be conducted to ensure treatment specificity. Additionally, developing nanocarriers with active targeting capabilities will help improve treatment precision. Finally, exploring the combined application of miR-193a-5p-Fe_3O_4 NPs with conventional chemotherapy or immune checkpoint inhibitors may yield synergistic anti-tumor effects, holding significant value for clinical translation.

CONCLUSION

This study confirms that miR-193a-5p-Fe_3O_4 NPs can effectively induce pyroptosis in gastric cancer cells by inhibiting the TGF-β1/Smad signaling pathway, thereby significantly suppressing tumor cell proliferation and migration. The composite material demonstrated a notable synergistic anti-tumor effect when combined with the TGF-β pathway inhibitor SB431542. Additionally, the study highlights the unique advantages of nanocarriers in enhancing miRNA stability and delivery efficiency. These findings establish an experimental foundation for the further development of novel gastric cancer treatment strategies integrating nanotechnology and gene regulation, holding significant translational medical value.

Acknowledgment
We gratefully acknowledge the Jiayuguan Traditional Chinese Medicine for providing the necessary equipment for this study.

Authors' contribution
All authors participated in the completion of the manuscript. Ziqin Chen and Huijuan Yu were responsible for drafting the manuscript, while Ye Lu and Xiaoshuang Du provided the overarching direction and guidance

Funding
None

Data availability statement
The datasets generated during and/or analysed during the current study are available from the corresponding author on reasonable request.

Ethical approval
This study utilized the commercially available human gastric cancer cell line MKN28. As the research did not involve any direct experiments on human participants or animals, no ethical approval from an institutional review board or ethics committee was required.

Disclaimers
The views and conclusions expressed in this article are solely those of the authors and do not necessarily represent the views of their affiliated institutions. The authors are responsible for the accuracy and completeness of the information provided, but do not accept any liability for any direct or indirect loss resulting from the use of this content.

Conflict of interest
The authors declare that they have no known competing financial interests or personal relationships that could have appeared to influence the work reported in this paper.

Informed consent
This article does not contain any studies on human or animal subjects.

REFERENCES

Albalawi AE, Khalaf AK, Alyousif MS, Alanazi AD, Baharvand P, Shakibaie M and Mahmoudvand H (2021). Fe3O4@piroctone olamine magnetic nanoparticles: Synthesize and therapeutic potential in cutaneous leishmaniasis. *Biomed Pharmacother*., **139**: 111566.

Baghbanzadeh A, Baghbani E, Hajiasgharzadeh K, Noorolyai S, Khaze V, Mansoori B, Shirmohamadi M, Baradaran B and Mokhtarzadeh A (2022). microRNA-193a-5p suppresses the migratory ability of human KATO III gastric cancer cells through inhibition of Vimentin and MMP-9. *Adv Pharm Bull*., **12**(1): 169–175.

Carpi S, Polini B, Manera C, Digiacomo M, Salsano JE, Macchia M, Scoditti E and Nieri P (2020). miRNA Modulation and antitumor activity by the extra-Virgin olive oil Polyphenol oleacein in human melanoma cells. *Front Pharmacol*., **11**: 574317.

Diener C, Keller A and Meese E (2022). Emerging concepts of miRNA therapeutics: From cells to clinic. *Trends Genet*., **38**(6): 613–626.

Feng M, Qin B, Luo F, Zhu X, Liu K, Li K, Wu D, Chen, G and Tang X (2024). Qingjie Huagong decoction inhibits pancreatic acinar cell pyroptosis by regulating circHipk3/miR-193a-5p/NLRP3 pathway. *Phytomedicine*., **126**: 155265.

Gokduman K and Gok A (2020). *In-vitro* Investigation of therapeutic potential of bare magnetite (Fe_3O_4) nanoparticles (≤100 ppm) on hepatocellular carcinoma cells. *J Nanosci Nanotechnol*., **20**(3): 1391–1400.

Han F, Zhou L, Zhao L, Wang L, Liu L, Li H, Qiu J, He J and Liu N (2021). Identification of miRNA in sheep intramuscular fat and the role of miR-193a-5p in proliferation and differentiation of 3T3-L1. *Front Genet*., **12**: 633295.

Hill M and Tran N (2021). miRNA interplay: Mechanisms and consequences in cancer. *Dis Model Mech*., **14**(4): 047662.

Mehta KJ (2022). Iron oxide nanoparticles in mesenchymal stem cell detection and therapy. *Stem Cell Rev Rep*., **18**(7): 2234–2261.

Pashirzad M, Khorasanian R, Fard MM, Arjmand MH, Langari H, Khazaei M, Soleimanpour S, Rezayi M, Ferns GA, Hassanian SM and Avan A (2021). The therapeutic potential of MAPK/ERK inhibitors in the treatment of colorectal cancer. *Curr Cancer Drug Targets*., **21**(11): 932–943.

Peng D, Fu M, Wang M, Wei Y and Wei X (2022). Targeting TGF-β signal transduction for fibrosis and cancer therapy. *Mol Cancer*., **21**(1): 104.

Piro NS, Hamad SM, Mohammed AS and Barzinjy AA (2023). Green synthesis magnetite (Fe_3O_4) nanoparticles from Rhus coriaria extract: A characteristic comparison with a conventional chemical method. *IEEE Trans Nanobioscience*., **22**(2): 308–317.

Qi X, Yao M, Jin M and Guo H (2021). Application of magnetic resonance imaging based on fe_3o_4 nanoparticles in the treatment of cerebrovascular diseases. *J Nanosci Nanotechnol*., **21**(2): 843–851.

Rouhani P and Singh RN (2020). Polyethyleneimine-functionalized magnetic Fe_3O_4 and nanodiamond particles as a platform for amoxicillin delivery. *J Nanosci Nanotechnol*., **20**(7): 3957–3970.

Sun H, Yan J, Tian G, Chen X and Song W (2021). LINC01224 accelerates malignant transformation via MiR-193a-5p/CDK8 axis in gastric cancer. *Cancer Med*., **10**(4): 1377–1393.

Wang J, Hu K, Cai X, Yang B, He Q, Wang J and Weng Q (2022). Targeting PI3K/AKT signaling for treatment of idiopathic pulmonary fibrosis. *Acta Pharm Sin B*., **12**(1): 18–32.

Wang Y, Li N, Zhao J and Dai C (2022). MiR-193a-5p serves as an inhibitor in ovarian cancer cells through RAB11A. *Reprod Toxicol*., **110**: 105–112.

Wen X, Jiao L and Tan H (2022). MAPK/ERK Pathway as a central regulator in vertebrate organ regeneration. *Int J Mol Sci*., **23**(3): 1464.

Xiang D, Zou J, Zhu X, Chen X, Luo J, Kong L and Zhang H (2020). Physalin D attenuates hepatic stellate cell activation and liver fibrosis by blocking TGF-β/Smad and YAP signaling. *Phytomedicine*., **78**: 153294.

Yu B, Luo F, Sun B, Liu W, Shi Q, Cheng SY, Chen C, Chen G, Li Y and Feng H (2021). KAT6A Acetylation of SMAD3 regulates myeloid-derived suppressor cell recruitment, metastasis and immunotherapy in triple-negative breast cancer. *Adv. Sci. (Weinh)*., **8**(20): e2100014.

Zhang J, Liu X, Wan C, Liu Y, Wang Y, Meng C, Zhang Y and Jiang C (2020). NLRP3 inflammasome mediates M1 macrophage polarization and IL-1β production in inflammatory root resorption. *J Clin Periodontol*. **47**(4): 451–460.

Zhang T, Xia W, Song X, Mao Q, Huang X, Chen B, Liang Y, Wang H, Chen Y, Yu X, Zhang Z, Yang W, Xu L, Dong G and Jiang F (2022). Super-enhancer hijacking LINC01977 promotes malignancy of early-stage lung adenocarcinoma addicted to the canonical TGF-β/SMAD3 pathway. *J Hematol Oncol*., **15**(1): 114.

Zhang X, Chen Y, Li Z, Han X and Liang Y (2020). TGFBR3 is an independent unfavourable prognostic marker in oesophageal squamous cell cancer and is positively correlated with Ki-67. *Int. J. Exp. Pathol*., **101**(6): 223–229.